

# Infection-induced Cascading Failures – Impacts and Mitigations

Bo Li<sup>1,2,\*</sup> and David Saad<sup>2,†</sup>

<sup>1</sup>*School of Science, Harbin Institute of Technology (Shenzhen), Shenzhen, 518055, China*

<sup>2</sup>*Non-linearity and Complexity Research Group, Aston University, Birmingham, B4 7ET, United Kingdom*

Coupled spreading processes on interdependent networks are studied, where the spreading infection of diseases or malware in one layer can trigger cascading failures in another layer and lead to secondary disasters, e.g., disrupting public services, supply chains, or power distribution. We utilize the dynamic message-passing method to devise efficient algorithms for inferring the system states, which allows one to investigate systematically the nature of such complex intertwined spreading processes and evaluate their impact. Based on the dynamic message-passing framework and optimal control, we further develop an effective optimization algorithm for mitigating network failures.

## I. INTRODUCTION

Epidemic outbreaks do not only possess a direct threat to public health but also, indirectly, impact other sectors [1–3]. For instance, when many infected individuals have to rest, be hospitalized or quarantined in order to slow down the epidemic spread, this could severely disrupt public services, causing disutility even to those who are not infected. For instance, the highly interdependent supply chains can be easily disrupted due to epidemic outbreaks [4, 5]. Similar concerns apply to cyber security. The spread of malware is not merely detrimental to computer networks, but can also cause failures to power grids or urban transportation networks which rely on modern communication systems [6, 7]. What is even worse is that the failures of certain components of technological networks can by themselves trigger a cascade of secondary failures, which can eventually lead to large-scale outages [8]. Therefore, it is vital to understand the nature of epidemic (or malware) spreading and failure propagation on interdependent networks, based on which, further mitigation and control measures can be devised.

A number of previous papers address the scenario of coupled spreading processes. In the context of epidemic spreading, two types of pathogens can cooperate or compete with each other, creating many intricate patterns of disease propagation [9–12]. For interdependent technological networks (e.g., a communication network coupled with a power network), the failure of components in one network will not only affect neighboring parts within the same network, but will also influence the adjoint network through the interdependent connections. Macroscopic analyses based on simplified models show that such a spreading mechanism can easily result in a catastrophic breakdown of the whole system [13, 14].

In this work, we study a scenario where the epidemic or malware spreading on one network can trigger cascading failures on another. This is highly relevant in the above-mentioned cases where epidemic outbreaks cause

disruption in public services or economic activities. Similarly, it can also be applied to study the effect of malware spread on computer networks causing the breakdown of other technological networks such as the power grid. The latter phenomenon is gaining more and more attention due to the increasing interdependency among various engineering networks [7].

Most existing research in the area of multi-layer spreading processes employs macroscopic approaches, such as the degree-distribution-based mean-field methods and asymptotic percolation analysis, in order to obtain the global picture of the models' behavior [15]. Such methods typically do not consider specific network instances and lack the ability to treat the interplay between the spreading dynamics and the fine-grained network topology [15]. For stochastic spreading processes with specific system conditions (e.g., topology initial conditions and individual node properties), it is common to apply extensive Monte Carlo (MC) simulations to observe the evolution of the spread, based on which important policy decisions are made [16]. However, such simulations are computationally demanding on big networks and can be subject to large statistical uncertainty; as a result, they are difficult to be used for downstream analysis or optimization tasks. Therefore, researchers have been pursuing tractable and accurate theoretical methods to tackle the complex stochastic dynamics on networks [15, 17].

Among the various developed theoretical approaches used, dynamic message-passing (DMP) is based on ideas from statistical physics offering a desirable algorithmic framework for approximate inference while it remains computationally efficient [18–20]. Notably, the DMP method has been shown to be much more accurate than the widely adopted individual-based mean-field method, especially in sparse networks [21, 22]. Moreover, the DMP approach yields a set of closed-form equations, which is very convenient for additional parameter estimation and optimization tasks [12, 23, 24]. In this work, we will leverage the DMP method to study the nature of infection-induced cascading failures, evaluate their impacts, and devise optimization algorithms for mitigating the failures. The remainder of the paper is organized as follows. We introduce the model and derive its DMP

\* libo2021@hit.edu.cn

† d.saad@aston.ac.uk

equations in Sec. II and Sec. III. We then investigate the impact of the spreading processes in Sec. IV, and devise optimization algorithms for mitigating the network failures in Sec. V. Finally, we summarize our findings and conclude the paper in Sec. VI.

## II. MODEL AND FRAMEWORK

### A. The Model

To study the impact of infection spread of diseases of malware and their secondary effects, we consider multi-layer networks comprising two layers [25], which are denoted as layers  $a$  and  $b$ , and are represented by two graphs  $G_a(V_a, E_a)$  and  $G_b(V_b, E_b)$ . For convenience, we assume that the nodes in both layers correspond to the same set of individuals, denoted as  $V = V_a = V_b$ . This can be extended to more general settings. Denote  $\partial_i^a$  and  $\partial_i^b$  as the sets of nodes adjacent to node  $i$  in layers  $a$  and  $b$ , respectively. We also define  $\partial_i = \partial_i^a \cup \partial_i^b$ . See Fig. 1 for an example of the network model under consideration.

Every individual has two states on layers  $a$  and  $b$ , respectively. In layer  $a$ , each node assumes one of four states, susceptible ( $S$ ), infected ( $I$ ), recovered ( $R$ ), and protected ( $P$ ) at any particular time step. The infection spreading process occurs in layer  $a$ , which is modeled by the stochastic discrete-time SIR model [15], augmented with a protection mechanism, which we term the SIRP model

$$\begin{aligned} S(i) + I(j) &\xrightarrow{\beta_{ji}} I(i) + I(j), \\ I(i) &\xrightarrow{\mu_i} R(i), \\ S(i) &\xrightarrow{\gamma_i(t)} P(i), \end{aligned} \quad (1)$$

where  $\beta_{ji}$  is the probability that node  $j$  being in the infected state transmits the infection to its susceptible neighboring node  $i$  at a certain time step. At each time step, an existing infected node  $i$  recovers with probability  $\mu_i$ ; the recovery process is assumed to occur after possible transmission activities. At time  $t$ , an existing susceptible node  $i$  turns into state  $P$  if it receives protection at time  $t-1$ , which occurs with probability  $\gamma_i(t-1)$ . The protection can be achieved by vaccination in the epidemic setting or special protection measures in the malware spread setting, which is usually subject to certain budget constraints. The protection probabilities  $\{\gamma_i(t)\}$  will be the major control variables for mitigating the outbreaks. At initial time  $t=0$ , we assume that node  $i$  has a probability  $P_S^i(0)$  to be in state  $S$ , and probability  $P_I^i(0) = 1 - P_S^i(0)$  to be in state  $I$ .

In layer  $b$ , each node  $i$  can either be in the normal state ( $N$ ) or the failed state ( $F$ ), indicated by a binary state variable  $x_i$  where  $x_i = 1$  (0) denotes the ‘fail’ (‘normal’) state at a particular time step. A node  $i$  in layer  $b$  fails if (i) it has been infected, i.e., node  $i$  is in state  $I$  or  $R$  in layer  $a$ ; (ii) there exists certain neighboring failed nodes

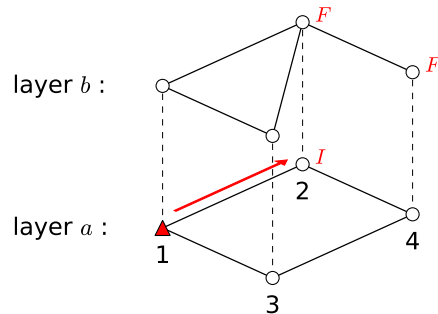


Figure 1. An example of the network model and the coupled spreading processes considered in this work. Node 2 is infected by node 1 in layer  $a$ , therefore it turns into state  $F$  in layer  $b$ . If  $b_{24} \geq \Theta_4$ , then node 4 will also fail as it loses the support from node 2, even though node 4 itself has not been infected.

such that  $\sum_{j \in \partial_i^b} b_{ij} x_j \geq \Theta_i$ , where  $\Theta_i$  is a threshold and the influence parameter  $b_{ij}$  measures the importance of the failure of node  $j$  on node  $i$ . The latter case indicates that node  $i$  can fail due to the failures of its neighbors which it relies on, even though node  $i$  itself is not infected. In summary, the failure propagation process in layer  $b$  can be expressed as

$$x_i = \begin{cases} 1, & \text{either (i) node } i \text{ in state } I \text{ or } R \text{ in layer } a, \\ & \text{or (ii) } \sum_{j \in \partial_i^b} b_{ij} x_j \geq \Theta_i \text{ in layer } b; \\ 0, & \text{otherwise.} \end{cases} \quad (2)$$

The whole process is simulated for  $T$  time steps. As we are interested in the time scale of infection spread which is usually very fast, we do not consider any repair rule in layer  $b$ . Therefore, a failed node cannot return to normality within the time window under consideration.

Such a failure propagation mechanism is equivalent to the linear threshold model (LTM) widely used in studying complex contagion in social networks [15, 26, 27]. Similar coupled SIR (without a protection mechanism) and LTM processes have also been considered in the social contagion setting [28].

Fig. 1 illustrates the infection-induced cascades in a simple network of 4 nodes. Node 1 is the initial infected node (or the seed) in layer  $a$ , which transmits the infection to node 2 at a certain time step. Now that node 2 is in the infected state in layer  $a$ , it also fails to function in layer  $b$ . If  $b_{24} \geq \Theta_4$ , then node 4 will also fail as it loses the support from node 2, even though node 4 itself has not been infected. Such additional cascade propagation needs extra care when infections spread out.

## B. The DMP Framework

We aim to use the DMP approach to investigate the coupled spreading processes described above. The DMP equations of the usual SIR and the LTM model have been derived, based on the microscopic dynamic belief propagation equations [20, 29]. As in generic belief propagation methods [30], the DMP method is exact on tree graphs, while it can constitute a good approximation in loopy graphs when short loops are scarce.

The coupled spreading processes combining the SIR and LTM model appear more involved, where approximations relying on uncorrelated multiplex networks were used [28]. Such approximations become less adequate when the two network layers are correlated, e.g., both layers share the same network topology.

## C. Dynamic Belief Propagation

To devise more accurate DMP equations for general network models and accommodate the protection mechanism for mitigation, we start from the principled dynamic belief propagation equations of the coupled process, instead of considering each process separately. One important characteristic of our model is that state transition is unidirectional, which can only take the direction  $S \rightarrow I \rightarrow R$  or  $S \rightarrow P$  in layer  $a$ , and  $N \rightarrow F$  in layer  $b$ . In this case, the DMP formalism is much more tractable [20].

Following Refs. [20, 29], we parametrize the dynamical trajectory of each node by its state transition times. In layer  $a$ , we denote  $\tau_i^a, \omega_i^a$  and  $\varepsilon_i^a$  as the first time at which node  $i$  turns into state  $I, R$  and  $P$ , respectively. In layer  $b$ , we denote  $\tau_i^b$  as the first time at which node  $i$  turns into state  $F$ . The cavity probability of the trajectory of node  $i$  in the absence of node  $j$ , denoted as  $m^{i \rightarrow j}(\tau_i^a, \omega_i^a, \varepsilon_i^a, \tau_i^b)$ , is computed by the following dynamic belief propagation equations

$$\begin{aligned} & m^{i \rightarrow j}(\tau_i^a, \omega_i^a, \varepsilon_i^a, \tau_i^b) \\ &= \sum_{\{\tau_k^a, \omega_k^a, \varepsilon_k^a, \tau_k^b\}_{k \in \partial_i^a}} W_{\text{SIRP}}^i(\tau_i^a, \omega_i^a, \varepsilon_i^a | \{\tau_k^a, \omega_k^a, \varepsilon_k^a\}_{k \in \partial_i^a}) \\ & \times W_{\text{LTM}}^i(\tau_i^b | \tau_i^a, \varepsilon_i^a, \{\tau_k^b\}_{k \in \partial_i^b}) \\ & \times \prod_{k \in \partial_i \setminus j} m^{k \rightarrow i}(\tau_k^a, \omega_k^a, \varepsilon_k^a, \tau_k^b), \end{aligned} \quad (3)$$

where  $W_{\text{SIRP}}^i(\cdot)$  and  $W_{\text{LTM}}^i(\cdot)$  are the transition kernels dictated by the dynamical rules of the SIRP and LTM model, respectively (for details see Appendix A). The marginal probability of the trajectory of node  $i$ , denoted as  $m^i(\cdot)$ , can be computed in a similar way as Eq. (3), by replacing the product  $\prod_{k \in \partial_i \setminus j}$  in the last line of Eq. (3) by  $\prod_{k \in \partial_i}$ .

The node-level probability of node  $i$  in a certain state can be computed by summing the trajectory-level probability, which will be described in the next section.

## III. NODE-LEVEL DMP EQUATIONS

Consider the cavity probability of node  $i$  being in state  $S$  in layer  $a$  at time  $t$  (assuming node  $j$  is absent - the cavity), it is obtained by tracing over the corresponding probabilities of trajectories  $m^{i \rightarrow j}(\cdot)$  in the cavity graph (assuming node  $j$  is removed)

$$\begin{aligned} P_S^{i \rightarrow j}(t) &= \sum_{\tau_i^a, \omega_i^a, \varepsilon_i^a, \tau_i^b} \mathbb{I}(t < \tau_i^a < \omega_i^a) \mathbb{I}(t < \varepsilon_i^a) \\ & \times m^{i \rightarrow j}(\tau_i^a, \omega_i^a, \varepsilon_i^a, \tau_i^b), \end{aligned} \quad (4)$$

where  $\mathbb{I}(\cdot)$  is the indicator function enforcing the order of state transitions. Similarly, we denote the cavity probability of node  $i$  in state  $F$  in layer  $b$  (in the absence of node  $j$ ) as  $P_F^{i \rightarrow j}(t)$ ; it is obtained by

$$P_F^{i \rightarrow j}(t) = \sum_{\tau_i^a, \omega_i^a, \varepsilon_i^a, \tau_i^b} \mathbb{I}(\tau_i^b \leq t) m^{i \rightarrow j}(\tau_i^a, \omega_i^a, \varepsilon_i^a, \tau_i^b). \quad (5)$$

The marginal probabilities  $P_S^i(t)$  and  $P_F^i(t)$  can be computed in a similar manner, by replacing  $m^{i \rightarrow j}(\cdot)$  in Eq. (4) and Eq. (5) with  $m^i(\cdot)$ .

### A. DMP Equations in Layer $a$

We note that infection spread in layer  $a$  is not influenced by cascades in layer  $b$ , while the failure time in layer  $b$  depends on the infection time and the protection time of the corresponding node in layer  $a$ . Hence, we can decompose the message  $m^{i \rightarrow j}(\cdot)$  to the respective components as

$$\begin{aligned} m^{i \rightarrow j}(\tau_i^a, \omega_i^a, \varepsilon_i^a, \tau_i^b) &= m_a^{i \rightarrow j}(\tau_i^a, \omega_i^a, \varepsilon_i^a) \\ & \times m_b^{i \rightarrow j}(\tau_i^b | \tau_i^a, \varepsilon_i^a). \end{aligned} \quad (6)$$

where  $m_a^{i \rightarrow j}(\cdot)$  and  $m_b^{i \rightarrow j}(\cdot)$  denote the trajectory-level probabilities of the processes in layer  $a$  and  $b$ , respectively.

Summing  $m_a^{i \rightarrow j}(\cdot)$  over  $\tau_i^a, \omega_i^a, \varepsilon_i^a$  up to a certain time yields the normal DMP equations of node-level probabilities for the infection spread in layer  $a$  (see details in Appendix A). They admit the following expressions for  $t > 0$

$$P_S^{i \rightarrow j}(t) = P_S^i(0) \prod_{t'=0}^{t-1} [1 - \gamma_i(t')] \prod_{k \in \partial_i \setminus j} \theta^{k \rightarrow i}(t), \quad (7)$$

$$\theta^{k \rightarrow i}(t) = \theta^{k \rightarrow i}(t-1) - \beta_{ki} \phi^{k \rightarrow i}(t-1), \quad (8)$$

$$\begin{aligned} \phi^{k \rightarrow i}(t) &= (1 - \beta_{ki})(1 - \mu_k) \phi^{k \rightarrow i}(t-1) \\ & - \left\{ P_S^{k \rightarrow i}(t) - P_S^{k \rightarrow i}(t-1)[1 - \gamma_k(t-1)] \right\}, \end{aligned} \quad (9)$$

where  $\theta^{k \rightarrow i}(t)$  is the cavity probability that node  $k$  has not transmitted the infection signal to node  $i$  up to time

$t$ , and  $\phi^{k \rightarrow i}(t)$  is the cavity probability that  $k$  is in state  $I$  but has not transmitted the infection signal to node  $i$  up to time  $t$ .

At time  $t = 0$ , as we consider that each node  $i$  is either in state  $S$  with probability  $P_S^i(0)$  or in state  $I$  with probability  $1 - P_S^i(0)$ , we have the following initial conditions for the messages

$$\begin{aligned} P_S^{i \rightarrow j}(0) &= P_S^i(0), \\ \phi^{i \rightarrow j}(0) &= 1 - P_S^i(0), \\ \theta^{i \rightarrow j}(0) &= 1. \end{aligned} \quad (10)$$

Upon iterating the above messages (7)-(9) starting from the initial conditions (10), the node-level marginal probabilities can be computed as

$$P_S^i(t) = P_S^i(0) \prod_{t'=0}^{t-1} [1 - \gamma_i(t')] \prod_{k \in \partial i} \theta^{k \rightarrow i}(t), \quad (11)$$

$$P_R^i(t) = P_R^i(t-1) + \mu_i P_I^i(t-1), \quad (12)$$

$$P_P^i(t) = P_P^i(t-1) + \gamma_i(t-1) P_S^i(t-1), \quad (13)$$

$$P_I^i(t) = 1 - P_S^i(t) - P_R^i(t) - P_P^i(t). \quad (14)$$

The above DMP equations (11)-(14) bear similarity to those of SIR model [19], except for the protection mechanism with control parameters  $\{\gamma_i(t)\}$ .

## B. DMP Equations in Layer $b$

As for the cascade process in layer  $b$ , whether node  $i$  will turn into state  $F$  (fail) also depends on the state in layer  $a$ , making it more challenging to derive the corresponding DMP equations. The key to obtaining node-level equations for  $P_F^{i \rightarrow j}(t)$  in Eq. (5) (and the corresponding marginal probability  $P_F^i(t)$ ) is to introduce several intermediate quantities to facilitate the calculation; the details are outlined in Appendix A.

To summarize, the node-level failure probability  $P_F^i(t)$  can be decomposed as

$$P_F^i(t) = P_I^i(t) + P_R^i(t) + P_{SF}^i(t) + P_{PF}^i(t), \quad (15)$$

where  $P_{SF}^i(t)$  and  $P_{PF}^i(t)$  are the probabilities that node  $i$  is in state  $F$  in layer  $b$ , while it is in state  $S$  or state  $P$  in layer  $a$ , respectively. For these two cases, the failure of node  $i$  is triggered by the failure propagation of its neighbors from layer  $b$ . A similar relation holds for the cavity probability  $P_F^{i \rightarrow j}(t)$ .

The probability  $P_{SF}^i(t)$  admits the following iteration

$$\begin{aligned} P_{SF}^i(t) &= P_S^i(0) \prod_{t'=0}^{t-1} [1 - \gamma_i(t')] \prod_{k \in \partial_i^a \setminus \partial_i^a \cap \partial_i^b} \theta^{k \rightarrow i}(t) \\ &\times \sum_{\{x_k\}_{k \in \partial_i^b}} \mathbb{I} \left( \sum_{k \in \partial_i^b} b_{ki} x_k \geq \Theta_i \right) \\ &\times \prod_{\substack{k \in \partial_i^b \setminus \partial_i^a \cap \partial_i^b, \\ x_k=1}} P_F^{k \rightarrow i}(t-1) \prod_{\substack{k \in \partial_i^b \setminus \partial_i^a \cap \partial_i^b, \\ x_k=0}} [1 - P_F^{k \rightarrow i}(t-1)] \\ &\times \prod_{\substack{k \in \partial_i^a \cap \partial_i^b, \\ x_k=1}} \chi^{k \rightarrow i}(t) \prod_{\substack{k \in \partial_i^a \cap \partial_i^b, \\ x_k=0}} [\theta^{k \rightarrow i}(t) - \chi^{k \rightarrow i}(t)], \end{aligned} \quad (16)$$

where  $\chi^{k \rightarrow i}(t)$  is the cavity probability that node  $k$  is in state  $F$  at time  $t-1$ , and it has not sent the infection signal to node  $i$  up to time  $t$ .

The cavity probability  $\chi^{k \rightarrow i}(t)$  can be decomposed into

$$\chi^{k \rightarrow i}(t) = \psi^{k \rightarrow i}(t) + P_{SF}^{k \rightarrow i}(t-1) + P_{PF}^{k \rightarrow i}(t-1), \quad (17)$$

where  $\psi^{k \rightarrow i}(t)$  is the cavity probability that node  $k$  is in state  $I$  or  $R$  at time  $t-1$ , but has not transmitted the infection signal to node  $i$  up to time  $t$ . The cavity probability  $\psi^{k \rightarrow i}(t)$  can be computed as

$$\begin{aligned} \psi^{k \rightarrow i}(t) &= \psi^{k \rightarrow i}(t-1) - \beta_{ki} \phi^{k \rightarrow i}(t-1) \\ &+ [1 - \gamma_k(t-2)] P_S^{k \rightarrow i}(t-2) - P_S^{k \rightarrow i}(t-1). \end{aligned} \quad (18)$$

Similarly, the probability  $P_{PF}^i(t)$  admits the following iteration

$$\begin{aligned} P_{PF}^i(t) &= P_S^i(0) \sum_{\varepsilon=1}^t \gamma_i(\varepsilon-1) \prod_{t'=0}^{\varepsilon-2} [1 - \gamma_i(t')] \\ &\times \prod_{k \in \partial_i^a \setminus \partial_i^a \cap \partial_i^b} \theta^{k \rightarrow i}(\varepsilon-1) \sum_{\{x_k\}_{k \in \partial_i^b}} \mathbb{I} \left( \sum_{k \in \partial_i^b} b_{ki} x_k \geq \Theta_i \right) \\ &\times \prod_{\substack{k \in \partial_i^b \setminus \partial_i^a \cap \partial_i^b, \\ x_k=1}} P_F^{k \rightarrow i}(t-1) \prod_{\substack{k \in \partial_i^b \setminus \partial_i^a \cap \partial_i^b, \\ x_k=0}} [1 - P_F^{k \rightarrow i}(t-1)] \\ &\times \prod_{\substack{k \in \partial_i^a \cap \partial_i^b, \\ x_k=1}} \tilde{\chi}^{k \rightarrow i}(t, \varepsilon) \prod_{\substack{k \in \partial_i^a \cap \partial_i^b, \\ x_k=0}} [\theta^{k \rightarrow i}(\varepsilon-1) - \tilde{\chi}^{k \rightarrow i}(t, \varepsilon)], \end{aligned} \quad (19)$$

where the dummy variable  $\varepsilon$  indicates the time at which node  $i$  receives the protection signal.

In Eq. (19),  $\tilde{\chi}^{k \rightarrow i}(t, \varepsilon)$  is the cavity probability that node  $k$  is in state  $F$  at time  $t-1$ , but has not transmitted the infection signal to node  $i$  up to time  $\varepsilon$ . It can be decomposed into

$$\tilde{\chi}^{k \rightarrow i}(t, \varepsilon) = \tilde{\psi}^{k \rightarrow i}(t, \varepsilon) + P_{SF}^{k \rightarrow i}(t-1) + P_{PF}^{k \rightarrow i}(t-1), \quad (20)$$

where  $\tilde{\psi}^{k \rightarrow i}(t, \varepsilon)$  is the cavity probability that node  $k$  is in state  $I$  or  $R$  at time  $t-1$ , but has not transmitted the

infection signal to node  $i$  up to time  $\varepsilon - 1$ . The cavity probability  $\psi^{k \rightarrow i}(t)$  can be computed as

$$\begin{aligned} \tilde{\psi}^{k \rightarrow i}(t, \varepsilon) &= \psi^{k \rightarrow i}(\varepsilon - 1) + P_I^{k \rightarrow i}(t - 1) + P_R^{k \rightarrow i}(t - 1) \\ &\quad - [P_I^{k \rightarrow i}(\varepsilon - 2) + P_R^{k \rightarrow i}(\varepsilon - 2)]. \end{aligned} \quad (21)$$

Note that the cavity probabilities  $P_{SF}^{i \rightarrow j}(t)$  and  $P_{PF}^{i \rightarrow j}(t)$  are computed using the similar formula as in Eq. (16) and Eq. (19), but in the cavity graph where node  $j$  is removed. This closes the loop for the DMP equations in layer  $b$ .

The initial conditions for the corresponding messages are given by

$$P_F^k(0) = P_F^{k \rightarrow i}(0) = P_I^k(0), \quad (22)$$

$$P_{SF}^k(0) = P_{SF}^{k \rightarrow i}(0) = 0, \quad (23)$$

$$P_{PF}^k(0) = P_{PF}^{k \rightarrow i}(0) = 0, \quad (24)$$

$$\psi^{k \rightarrow i}(1) = \chi^{k \rightarrow i}(1) = (1 - \beta_{ki})P_I^k(0), \quad (25)$$

$$\tilde{\psi}^{k \rightarrow i}(1, 1) = \tilde{\chi}^{k \rightarrow i}(1, 1) = P_I^k(0). \quad (26)$$

For  $t \geq 2, \varepsilon = 1$ , we have

$$\tilde{\psi}^{k \rightarrow i}(t, \varepsilon = 1) = P_I^{k \rightarrow i}(t - 1) + P_R^{k \rightarrow i}(t - 1), \quad (27)$$

$$\begin{aligned} \tilde{\chi}^{k \rightarrow i}(t, \varepsilon = 1) &= P_I^{k \rightarrow i}(t - 1) + P_R^{k \rightarrow i}(t - 1) \\ &\quad + P_{SA}^{k \rightarrow i}(t - 1) + P_{PA}^{k \rightarrow i}(t - 1). \end{aligned} \quad (28)$$

We remark that for a total time  $T$ , the computational complexity for the node-level DMP equations is of  $O(|E|T^2)$ , unlike the  $O(|E|T)$  complexity for the SIRP model. This is due to the coupling of the two-layer processes and the protection mechanism. The summation of the dummy state  $\{x_k\}_{k \in \partial_i^b}$  in Eq. (16) and Eq. (19) also implies a high computational demand of networks with high-degree nodes. One way to alleviate this complexity is to use the dynamic programming techniques introduced in Ref. [31].

These DMP equations are exact if both layers are tree networks, while they are approximate solutions when there are loops in the underlying networks.

### C. Simplification in the Absence of Neighbors Overlap

If there are no overlaps between the neighbors of node  $i$  in layer  $a$  and those in layer  $b$ , i.e.,  $\partial_i^a \cap \partial_i^b = \emptyset$ , the messages  $\chi^{k \rightarrow i}, \psi^{k \rightarrow i}, \tilde{\chi}^{k \rightarrow i}$  and  $\tilde{\psi}^{k \rightarrow i}$  are not needed, and the node-level probabilities  $P_{SF}^i(t)$  and  $P_{PF}^i(t)$  can be

much simplified as

$$\begin{aligned} P_{SF}^i(t) &= P_S^i(t) \sum_{\{x_k\}_{k \in \partial_i^b}} \mathbb{I} \left( \sum_{k \in \partial_i^b} b_{ki} x_k \geq \Theta_i \right) \\ &\quad \times \prod_{k \in \partial_i^b, x_k=1} P_F^{k \rightarrow i}(t - 1) \prod_{k \in \partial_i^b, x_k=0} [1 - P_F^{k \rightarrow i}(t - 1)], \end{aligned} \quad (29)$$

$$\begin{aligned} P_{PF}^i(t) &= P_P^i(t) \sum_{\{x_k\}_{k \in \partial_i^b}} \mathbb{I} \left( \sum_{k \in \partial_i^b} b_{ki} x_k \geq \Theta_i \right) \\ &\quad \times \prod_{k \in \partial_i^b, x_k=1} P_F^{k \rightarrow i}(t - 1) \prod_{k \in \partial_i^b, x_k=0} [1 - P_F^{k \rightarrow i}(t - 1)]. \end{aligned} \quad (30)$$

This is also a reasonable approximation if the two layers  $a$  and  $b$  have little correlation, which has been exploited in Ref. [28]. In this work, we will employ this approximation when we consider the dynamics in the large time limit and devise an optimization algorithm for mitigating the cascading failures, in order to reduce the computational complexity.

### D. Effectiveness of the DMP Method

We test the efficacy of the DMP equations derived in Sec. III A and Sec. III B, by comparing the node-level probabilities  $P_S^i(t)$  and  $P_F^i(t)$  to those obtained by Monte Carlo (MC) simulations. The DMP theory produces exact marginal probabilities for node activities in coupled tree networks, as demonstrated in Fig. 2(a) and (b). For random regular graphs where there are many loops, the DMP method also yields reasonably accurate solutions, as demonstrated in Fig. 2(c) and (d).

## IV. IMPACT OF INFECTION-INDUCED CASCADES

The obtained DMP equations of the coupled SIRP and LTM models allow us to examine the impact of the infection-induced cascading failures, on either a specific instance of a multiplex network or an ensemble of networks following a certain degree distribution. In this section, we do not consider the protection of nodes by setting  $\gamma_i(t) = 0$ , where the process in layer  $a$  is essentially a discrete-time SIR model.

### A. Impact on A Specific Network

For the process in layer  $a$ , we define the outbreak size at time  $t$  as the fraction of nodes that have been infected at that time

$$\rho_I + \rho_R = \frac{1}{N} \sum_{i \in V_a} P_I^i(t) + \frac{1}{N} \sum_{i \in V_a} P_R^i(t). \quad (31)$$



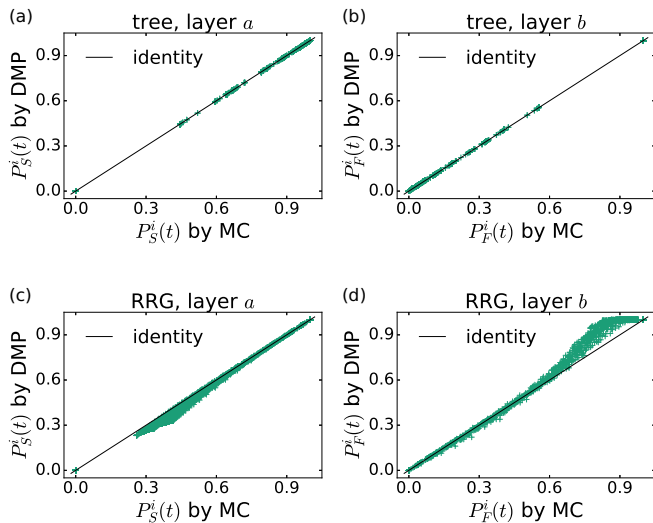


Figure 2. Comparison of node-level probabilities  $P_S^i(t)$  and  $P_F^i(t)$  obtained by the DMP theory and Monte Carlo simulation (averaged over  $10^5$  realizations). Panels (a) and (b) correspond to a binary tree network of size  $N = 63$  for both layers. Panels (c) and (d) correspond to a random regular graph (RRG) of size  $N = 100$  and degree  $K = 5$  for both layers. The system parameters are  $T = 50, \beta_{ij} = 0.2, \mu_i = 0.5, b_{ij} = 1, \Theta_i = 0.6|\partial_i^b|, \gamma_i(t) = 0$ .

For the process in layer  $b$ , we define the cascade size at time  $t$  as the fraction of nodes that have failed at that time

$$\rho_F = \frac{1}{N} \sum_{i \in V_b} P_F^i(t). \quad (32)$$

By definition, we have  $\rho_F \geq \rho_I + \rho_R$ .

In Fig. 3, we demonstrate the time evolution of the infection outbreak size and the cascade size in a multiplex network where both layers are random regular graphs with size  $N = 1600$ . It can be observed that  $\rho_F$  is much larger than  $\rho_I + \rho_R$  asymptotically, which suggests that the failure propagation mechanism in layer  $b$  significantly amplifies the impact of the infection outbreaks in layer  $a$ . In particular, the failure can eventually propagate to the whole network even though less than 70% of the population gets infected when the spread of the infection saturates. Compare to MC simulations, the DMP method systematically overestimates the outbreak sizes due to the effect of mutual infection, but it has been shown to offer a significant improvement over the individual-based mean-field method [21, 22, 32].

## B. Asymptotic Properties

In the above example, the system converges to a steady state in the large time limit. The DMP approach allows us to systematically investigate the asymptotic behavior of the coupled spreading processes.

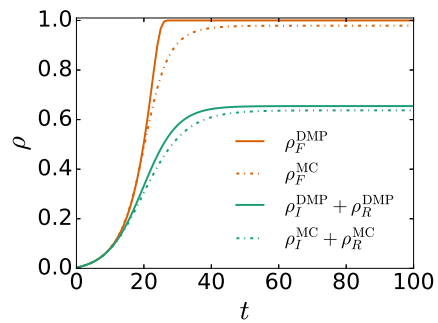


Figure 3. Evolution of the sizes of the infection outbreak in layer  $a$  (measured by  $\rho_I + \rho_R$ ) and total failures in layer  $b$  (measured by  $\rho_F$ ). Layer  $a$  and layer  $b$  have different network topologies, but both are realizations of random regular graphs of size  $N = 1600$  and degree  $K = 5$ . At time  $t = 0$ , there are 5 infected nodes. The system parameters are  $\beta_{ij} = 0.2, \mu_i = 0.5, b_{ij} = 1, \Theta_i = 0.6|\partial_i^b|, \gamma_i(t) = 0$ .

For the process in layer  $a$ , we define an auxiliary probability

$$p_{ij} := \frac{\beta_{ij}}{\beta_{ij} + \mu_i - \beta_{ij}\mu_i}. \quad (33)$$

Then the messages in layer  $a$  admit the following expressions in the limit  $T \rightarrow \infty$

$$\begin{aligned} \phi^{i \rightarrow j}(\infty) &= 0, \\ \theta^{i \rightarrow j}(\infty) &= 1 - p_{ij} + p_{ij} P_S^{i \rightarrow j}(\infty), \\ P_S^{i \rightarrow j}(\infty) &= P_S^i(0) \prod_{k \in \partial_i^a \setminus j} \theta^{k \rightarrow i}(\infty), \\ P_S^i(\infty) &= P_S^i(0) \prod_{k \in \partial_i^a} \theta^{k \rightarrow i}(\infty), \end{aligned} \quad (34)$$

Details of the derivation can be found in Appendix B. The above asymptotic equations (34) suggest a well-known relationship between epidemic spreading and bond percolation [15, 18, 33]. The quantity  $p_{ij}$  defined in Eq. (33) can be interpreted as a bond occupation probability of edge  $(i, j)$ , which differs from the continuous-time counterpart [18, 33] with an additional term  $\beta_{ij}\mu_i$  in the denominator. The term  $\beta_{ij}\mu_i$  accounts for the simultaneous events that node  $i$  infects node  $j$  and recovers within the same time step [21].

For the process in layer  $b$ , we assume that layers  $a$  and  $b$  are weakly correlated due to their different topologies and adopt the approximation made in Sec. III C. As no protection is applied, we have  $P_{P_F}^i(t) = 0$ . Then the messages in layer  $b$  admit the following expression in the

limit  $T \rightarrow \infty$

$$\begin{aligned}
P_F^{i \rightarrow j}(\infty) &= 1 - P_S^i(\infty) \\
&+ P_S^i(\infty) \sum_{\{x_k\}_{k \in \partial_i^b \setminus j}} \mathbb{I} \left( \sum_{k \in \partial_i^b \setminus j} b_{ki} x_k \geq \Theta_i \right) \\
&\times \prod_{k \in \partial_i^b \setminus j, x_k=1} P_F^{k \rightarrow i}(\infty) \prod_{k \in \partial_i^b \setminus j, x_k=0} [1 - P_F^{k \rightarrow i}(\infty)],
\end{aligned} \tag{35}$$

where a similar expression holds for  $P_F^i(\infty)$  by replacing  $\partial_i^b \setminus j$  with  $\partial_i^b$  in Eq. (35). The asymptotic equations for layer  $b$  suggest a relationship between the LTM model and bootstrap percolation [29].

### C. Coupled Percolation in Large Homogeneous Networks

The large-time behaviors of the two processes correspond to two types of percolation problems. To further examine the macroscopic critical behaviors of the coupled percolation models, it is convenient to consider large-size random regular graphs of degree  $K$  (which have a homogeneous network topology), and homogeneous system parameters with  $\beta_{ij} = \beta, \mu_i = \mu, b_{ij} = b, \Theta_i = \Theta$ . We further assume that each node  $i$  has a vanishingly small probability of being infected at time  $t = 0$  with  $P_I^i(0) = 1 - P_S^i(0) \propto 1/N$ . In the large size limit  $N \rightarrow \infty$ , we have  $P_S^i(0) \rightarrow 1$ .

Due to the homogeneity of the system, one can assume that all messages and marginal probabilities are identical,

$$\theta^{i \rightarrow j}(\infty) = \theta^\infty, \tag{36}$$

$$P_F^{i \rightarrow j}(\infty) = P_F^\infty, \tag{37}$$

$$P_S^i(\infty) = \rho_S^\infty, \tag{38}$$

$$P_F^i(\infty) = \rho_F^\infty. \tag{39}$$

It leads to the self-consistent equations in the large size limit ( $N \rightarrow \infty$ ),

$$\theta^\infty = 1 - p + p \cdot (\theta^\infty)^{K-1}, \tag{40}$$

$$\rho_S^\infty = (\theta^\infty)^K, \tag{41}$$

$$P_F^\infty = 1 - \rho_S^\infty \tag{42}$$

$$\begin{aligned}
&+ \rho_S^\infty \sum_{n=\lceil \Theta \rceil}^{K-1} \binom{K-1}{n} (P_F^\infty)^n (1 - P_F^\infty)^{K-1-n}, \\
\rho_F^\infty &= 1 - \rho_S^\infty
\end{aligned} \tag{43}$$

$$+ \rho_S^\infty \sum_{n=\lceil \Theta \rceil}^K \binom{K}{n} (P_F^\infty)^n (1 - P_F^\infty)^{K-n},$$

where  $p = \frac{\beta}{\beta + \mu - \beta \mu}$  and  $\lceil x \rceil$  is the smallest integer greater than or equal to  $x$ .

We observe that  $\theta^\infty = 1, \rho_S^\infty = 1, P_F^\infty = 0, \rho_F^\infty = 0$  is always a fixed point to Eqs. (40)-(43), which corresponds

to vanishing outbreak sizes. When the infection probability  $\beta$  is larger than a critical point  $\beta_c^a$ , this fixed point solution becomes unstable and another fixed point with finite outbreak sizes develops.

As a concrete example, we consider random regular graphs of degree  $K = 5$  and fix  $\mu = 0.5, b = 1, \Theta = 3$ . By solving Eqs. (40)-(43) for different  $\beta$ , we obtain outbreak sizes for both layers  $a$  and  $b$  under different infection strengths. The result is shown in Fig. 4, where the asymptotic theory accurately predicts the behavior of a large-size system ( $N = 1600$ ) in the large-time limit. It is also observed that the outbreak sizes in both layers become non-zero when  $\beta$  is larger than a critical point  $\beta_c^a = \frac{1}{7}$ . Furthermore, the outbreak size  $\rho_F^\infty$  in layer  $b$  exhibits a discontinuous jump to a complete breakdown ( $\rho_F^\infty = 1$ ) when  $\beta$  increases and surpasses another transition point  $\beta_c^b \approx 0.159$ . However, at the transition point  $\beta_c^b$ , only about 28.6% of the population has been infected in layer  $a$ .

This example again indicates that the cascading failure propagation in layer  $b$  can drastically amplify the impact of the epidemic outbreaks in layer  $a$ . Lastly, we remark that whether layer  $b$  will exhibit a discontinuous transition or not depends on the values of  $K$  and  $\Theta$  [29], as predicted by the bootstrap percolation theory [34].

## V. MITIGATION OF INFECTION-INDUCED CASCADES

### A. The Optimization Framework

The catastrophic breakdown can be mitigated if timely protections are provided to stop the infection's spread. In our model, this is implemented by assigning a non-zero protection probability  $\gamma_i(t)$  to node  $i$ , after which it is immune from infection from layer  $a$ . To minimize the size of final failures, it would be more effective to take into account the spreading processes in both layers  $a$  and  $b$  when deciding which nodes to prioritize for protection.

Here, we develop mitigation strategies by solving the following constrained optimization problems

$$\min_{\gamma} \mathcal{O}(\gamma) := \rho_F(T) = \frac{1}{N} \sum_{i \in V_b} P_F^i(T), \tag{44}$$

$$\text{s. t. } 0 \leq \gamma_i(t) \leq 1 \quad \forall i, t, \tag{45}$$

$$\sum_{i \in V_b} \sum_{t=0}^{T-1} \gamma_i(t) \leq \gamma^{\text{tot}}, \tag{46}$$

where the constraint in Eq. (45) ensures that  $\gamma_i(t)$  is a probability, and Eq. (46) represents the global budget constraint on the protection resources. As the objective function  $\mathcal{O}(\gamma)$  (the size of final failures) depends on the evolution of the coupled spreading processes, the optimization problem is challenging. Ref. [24] introduced the optimal control framework to tackle similar problems, by estimating the marginal probabilities of individuals with

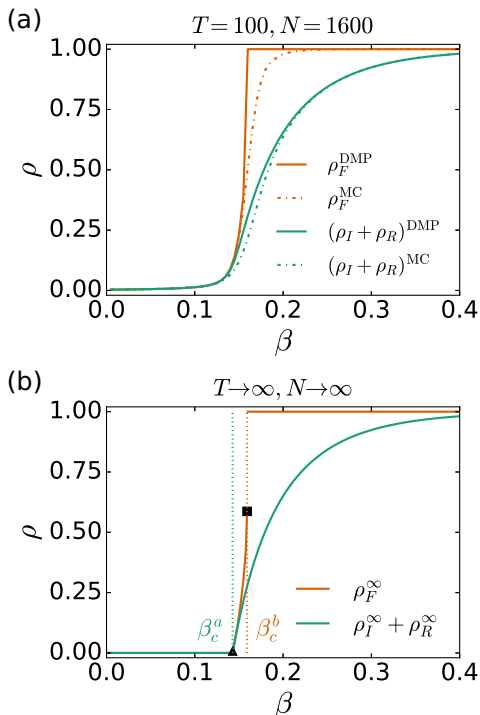


Figure 4. Size of infection outbreak in layer  $a$  (measured by  $\rho_I + \rho_R$ ) and total failures in layer  $b$  (measured by  $\rho_F$ ) as a function of the infection probability  $\beta$  in the large-time limit. (a) Random regular graphs with  $N = 1600, K = 5$  are considered. The spreading processes are iterated for  $T = 100$  steps, where stationary states are attained. (b) Random regular graphs with  $K = 5$  in the asymptotic limit  $T \rightarrow \infty, N \rightarrow \infty$  are considered by analyzing the large-time behaviors of the DMP equations. The triangle and the square markers indicate the locations of the two transition points  $\beta_c^a$  and  $\beta_c^b$ , respectively. The system parameters are homogeneous, with  $\mu = 0.5, b = 1, \Theta = 3, \gamma_i(t) = 0$ .

the DMP methods. The success of the optimal control approach highlights another advantage of the theoretical methods over numerical simulations [12, 24, 35].

In this work, we adopt a similar strategy to solve the optimization problem defined in Eqs. (44)-(46), where  $P_F^i(T)$  is estimated by the DMP equations derived in Sec. III. We also adopt the approximation made in Sec. III C for simplicity. As the expressions of the DMP equations have been explicitly given and only involve elementary arithmetic operations, we leverage tools of automatic differentiation to compute the gradient of the objective function  $\nabla_\gamma \mathcal{O}(\gamma)$  in a back-propagation fashion [36]. It allows us to derive gradient-based algorithms for solving the optimization problem. We remark that such a back-propagation algorithm is equivalent to optimal control with gradient descent update on the control parameters [37].

To handle the box constraint in Eq. (45), we adopt the mirror descent method, which performs the gradient-based update in the dual (or mirror) space rather than

the primal space where  $\{\gamma_i(t)\}$  live [38, 39]. In our case, we use the logit function  $\Psi(x) = \log(\frac{x}{1-x})$  to map the primal control variable  $\gamma_i(t)$  to the dual space as  $h_i(t) = \psi(\gamma_i(t)) \in \mathbb{R}$ , where the gradient descent updates are performed. The primal variable can be recovered through the inverse mapping of  $\Psi(\cdot)$ , which is  $\Psi^{-1}(h) = \frac{1}{1+\exp(-h)}$ . The elementary mirror descent update step is

$$g^n \leftarrow \nabla_\gamma \mathcal{O}(\gamma^n), \quad (47)$$

$$\gamma^{n+1} \leftarrow \Psi^{-1}(\Psi(\gamma^n) - sg^n), \quad (48)$$

where  $n$  is an index keeping track of the optimization process and  $s$  is the step size of the gradient update.

In general, the above optimization process tends to increase the total resources  $\sum_{i,t} \gamma_i(t)$ . To prevent the violation of the constraint in Eq. (46) during the updates, we suppress the gradient component which increases the total resources when  $\sum_{i,t} \gamma_i(t) \geq (1 - \epsilon)\gamma^{\text{tot}}$ , by shifting the gradient  $g^n$  in Eq. (48) with a magnitude  $b^n$

$$b^n \leftarrow \frac{\sum_{t,i} \gamma_i^n(t)(1 - \gamma_i^n(t)) \frac{\partial}{\partial \gamma_i(t)} \mathcal{O}(\gamma^n)}{\sum_{t,i} \gamma_i^n(t)(1 - \gamma_i^n(t))}, \quad (49)$$

$$g^n \leftarrow \nabla_\gamma \mathcal{O}(\gamma^n) - b^n. \quad (50)$$

The rationale for the choice of  $b^n$  is explained in Appendix C. In our implementation of the algorithm, we choose  $\epsilon = 0.02$ . Even though the shifted gradient method is used, it does not strictly forbid the violation of the constraint in Eq. (46). If the resource capacity constraint is violated, we project the control variables to the feasible region through the simple rescaling

$$\gamma^n \leftarrow \frac{\gamma^{\text{tot}}}{\sum_{t,i} \gamma_i^n(t)} \gamma^n. \quad (51)$$

Finally, the resource capacity constraint Eq. (46) implies that a  $\gamma^{\text{tot}}$  amount of protection resources can be distributed in different time steps. In some scenarios, the resources arrive in an online fashion, e.g., a limited number of vaccines can be produced every day. In these cases, there is a resource capacity constraint at each time step. Some results of such a scenario are discussed in Appendix D.

## B. Case Study on a Tree Network

We first verify the effectiveness of the optimization method by considering a simple problem on a binary tree network of size  $N = 63$ . Three individuals are chosen to be infected at time  $t = 0$ , and the outbreak is simulated for  $T = 50$  time steps. The system parameters are set as  $\beta_{ij} = 0.5, \mu_i = 0.5, b_{ij} = 1, \Theta_i = 0.6|\partial_i^b|$ . Without any mitigation strategy, *more than half of the population fail* at the end of the process.

We then protect some vital nodes to mitigate the system failure, by using the optimization method proposed



in Sec. V A. On the left column of Fig. 5, we restrict the total resource to be  $\gamma^{\text{tot}} = 5$ . Fig. 5(a) shows that the optimization algorithm successfully reduces the final failure rate, which demonstrates the effectiveness of the method. We found that the optimal protection resource distribution  $\{\gamma_i^*(t)\}$  mostly concentrates on a few nodes at a certain time step (as shown in Fig. 5(c)), which implies that we can confidently select which nodes to protect. All the nodes with high  $\gamma_i^*(t)$  receive protection at time  $t = 0$ , which implies that the best mitigation strategy in this example is to distribute all  $\gamma^{\text{tot}}$  resources as early as possible to stop the infection spread. Fig. 5(e) shows the optimal placement of resources, which can completely block the infection spread, hence minimizing the network failure. In this example, both layers  $a$  and  $b$  have the same network structure, which is depicted in Fig. 5(e).

Similar phenomena are observed in the case with  $\gamma^{\text{tot}} = 4$  as shown in the right column of Fig. 5, except that the protections are not sufficient to completely block the infection spread. The optimization algorithm sacrifices only two nodes in the vicinity of the infected node in the lower right corner of Fig. 5(f) (indicated by a black arrow), leaving other parts of the network in the normal state.

The good performance of the optimization is based on the fact that there are enough protection resources (i.e., having a large  $\gamma^{\text{tot}}$ ) as well as being aware of the origins of the outbreak. In some cases, whether a node was infected at the initial time is not fully determined but follows a probability distribution. Such cases can be easily accommodated in the DMP framework which is intrinsically probabilistic. We investigated such a scenario with probabilistic seeding in Appendix E, and found that the optimization method can still effectively reduce the sizes of network failures.

### C. Case Study in a Synthetic Network

To further showcase the applicability of the optimization algorithm for failure mitigation, we consider a synthetic technological multiplex network where layer  $a$  represents a communication network and layer  $b$  represents a power network. We consider the scenario that the communication network can be attacked by malware but can also be protected by technicians, which is modeled by the proposed SIRP model. The infection of a node in the communication network causes the breakdown of the corresponding node in the power network. The breakdown of components in a power network can trigger further failures and form a cascade, which is modeled by the proposed LTM model. We have neglected the details of the power flow dynamics in order to obtain a tractable model and an insightful simple example.

Here, we extract the network topology from the IEEE 118-bus test case to form layer  $b$  [40], which has  $N = 118$  nodes. We then obtain layer  $a$  by rewiring a regular graph of the same size with degree  $K = 4$  using a rewiring

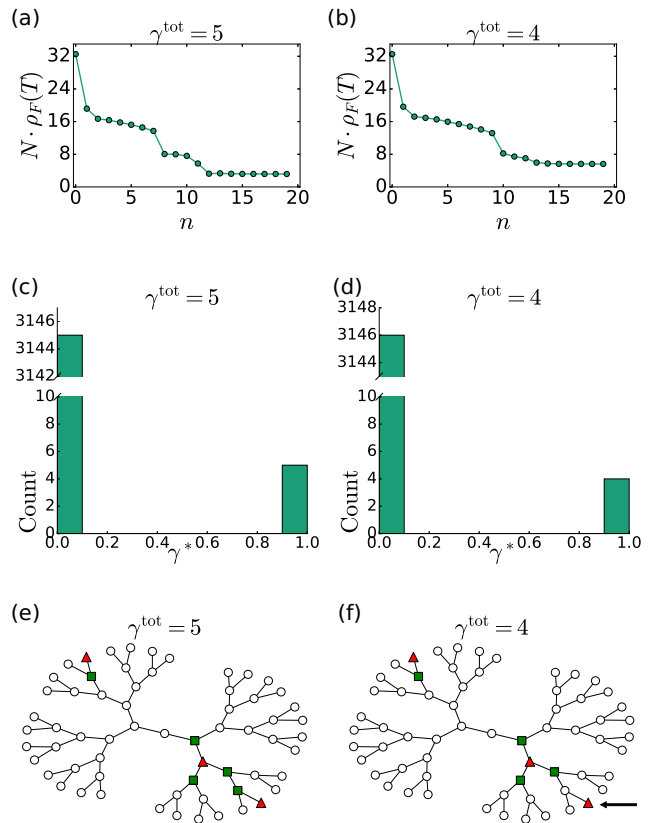


Figure 5. Mitigation of the network failures in a binary tree network of size  $N = 63$  for both layers. Panels (a)(c)(e) correspond to the case with  $\gamma^{\text{tot}} = 5$ , while Panels (b)(d)(f) correspond to the case with  $\gamma^{\text{tot}} = 4$ . Panels (a) and (b) depict how the final failure size changes during the optimization process. Specifically, the control parameters  $\{\gamma_i^n(t)\}$  for each optimization step  $n$  were recorded, which were fed to the DMP equations for computing  $\rho_F(T)$  at step  $n$ . Panels (c) and (d) plot the histogram of the optimal decision variables  $\{\gamma_i^*(t)\}$ . Panels (e) and (f) show the optimal placement of resources on layer  $a$ , where green square nodes receive protection (having a high  $\gamma_i^*(t)$  at time  $t = 0$ ). The three red triangle nodes are the initially infected individuals.

probability  $p_{\text{rewire}} = 0.3$ , which creates a Watts-Strogatz small-world network and mimics the topology of communication networks [41]. The resulting multiplex network is plotted in Fig. 6.

As the failures in layer  $b$  are initially induced by the infections in layer  $a$ , one may wonder whether deploying the protection resource by minimizing the size of infections, i.e., minimizing  $\rho_I(T) + \rho_R(T)$  instead of minimizing  $\rho_F(T)$ , is already sufficient to mitigate the final failures. To investigate this effect, we replace the objective function in Eq. (44) by  $\mathcal{O}^a(\gamma) = \rho_I(T) + \rho_R(T)$  and solve the optimization problem using the same techniques in Sec. V A. The result is shown in Fig. 7(a), which suggests that blocking the infection is as good as minimizing the original objective function in Eq. (44) for the purpose of minimizing the total failure size. Minimizing-

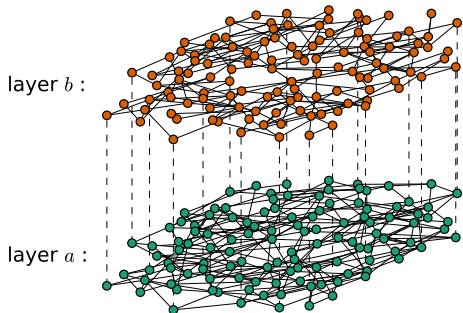


Figure 6. An artificial two-layer network, where each layer has  $N = 118$  nodes. Layer  $a$  is a Watts-Strogatz small-world network, which mimics the topology of communication networks; it is obtained by rewiring a regular graph of degree 4 with rewiring probability  $p_{\text{rewire}} = 0.3$ . Layer  $b$  is a power network extracted from the IEEE 118-bus test case.

ing either objective function constitutes a much better improvement over the random deployment of the same amount of protection resources in this case.

The results in Fig. 7(a) point to the conventional wisdom that one should try best to stop the epidemic or malware spread (in layer  $a$ ) for mitigating system failure. The situation will be different if there are vital components in layer  $b$ , which should be protected to prevent the failure cascade. This is typically manifested in the heterogeneity of the network connectivity or the system parameters. To showcase this effect, we manually plant a vulnerable connected cluster in layer  $b$  by setting the influence parameters  $b_{ji}$  for an edge  $(i, j)$  in this cluster as  $b_{ji} = \Theta_i$ , so that the failure of node  $i$  itself is already sufficient to trigger the failure of node  $j$ . In this case, we found that minimizing  $\rho_F(T)$  yields a much better improvement over minimizing  $\rho_I(T) + \rho_R(T)$  for the purpose of mitigating the system failure, as shown in Fig. 7(b).

## VI. CONCLUSION AND DISCUSSION

We investigate the nature of a type of coupled spreading processes in interdependent networks, comprising two interacting layers  $a$  and  $b$ . Disease or malware spreads in layer  $a$ , which can trigger cascading failures in layer  $b$ , leading to secondary disasters. The spreading processes in the two layers are modeled by the SIRP and LTM models, respectively. To tackle the complex stochastic dynamics in interdependent networks, we utilized the dynamic message-passing method by working out the dynamic belief propagation equations. The resulting DMP algorithms have low computational complexity and allow us to perform accurate and efficient inference of the system states.

Based on the DMP method, we systematically studied

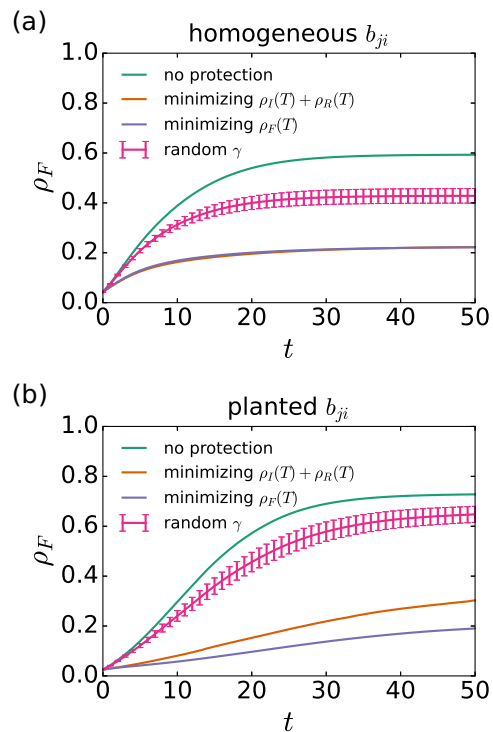


Figure 7. Evolution of the failure rate  $\rho_F(t)$  of the synthetic network shown in Fig. 6 under various mitigation strategies. The curve labeled by “random  $\gamma$ ” corresponds to the random deployment of a  $\gamma^{\text{tot}}$  amount of protection resources at time  $t = 0$ ; 20 different random realizations are considered and the error bar indicates one standard deviation of the sample fluctuations. The time window is set as  $T = 50$ . (a) Most system parameters are homogeneous with  $\beta_{ji} = 0.2$ ,  $\mu = 0.5$ ,  $b_{ji} = 1$ , while  $\Theta_i = 0.6|\partial_i^b|$ . Five nodes are randomly chosen as the initially infected individuals, and  $\gamma^{\text{tot}} = 10$  is considered. (b) The system parameters are  $\beta_{ji} = 0.17$ ,  $\mu = 0.5$ ,  $\Theta_i = 0.6|\partial_i^b|$ . Planted influence parameters  $\{b_{ji}\}$  are considered. Three nodes are randomly chosen as the initially infected individuals, and  $\gamma^{\text{tot}} = 9$  is considered.

and evaluated the impact of the infection-induced cascading failures. The cascade process in layer  $b$  can lead to large-scale network failures, even when the infection rate in layer  $a$  remains at a relatively low level. By considering a homogeneous network topology and homogeneous system parameters, we derive the asymptotic and large-size limits of the DMP equations. The asymptotic limit of the coupled spreading processes corresponds to the coupling between a bond percolation model and a bootstrap percolation model, which can be analytically solved. The infection outbreak size in layer  $a$  changes continuously from zero to non-zero as the infection probability  $\beta$  surpasses a transition point  $\beta_c^a$ , while the failure size in layer  $b$  can exhibit a discontinuous jump to the completely failed state when  $\beta$  surpasses another transition point  $\beta_c^b$  under certain conditions. All these results highlight the observation that cascading failure propagation in layer  $b$  can drastically amplify the impact of

the epidemic outbreaks in layer  $a$ , which requires special attention.

Another advantage of the DMP method is that it yields a set of closed-form equations, which can be very useful for other downstream analyses and tasks. We exploited this property to devise optimization algorithms for mitigating network failure. The optimization method works by back-propagating the impact at the final time to adjust the control parameters (i.e., the protection probabilities). The mirror descent method and a heuristic gradient shift method were also used to handle the constraints on the control parameter. We show that the resulting algorithm can effectively minimize the size of system failures. We believe that our dedicated analyses provide valuable insights and a deeper understanding of the impact the infection-induced cascading failures on networks, and the

obtained optimization algorithms will be useful for practical applications in systems of this kind.

## ACKNOWLEDGMENTS

B.L. and D.S. acknowledge support from European Union's Horizon 2020 research and innovation programme under the Marie Skłodowska-Curie Grant Agreement No. 835913. B.L. acknowledges support from the startup funding from Harbin Institute of Technology, Shenzhen (Grant No. 20210134), and the National Natural Science Foundation of China (Grant No. 12205066). D.S. acknowledges support from the Leverhulme Trust (RPG-2018-092) and the EPSRC programme grant TRANSNET (EP/R035342/1).

## Appendix A: Deriving the DMP Equations From Dynamic Belief Propagation

In this Appendix, we supplement some technical details of the DMP equations based on dynamic belief propagation.

We assume that at the initial time  $t = 0$ , node  $i$  is either in state  $S$  or state  $I$ , occurring with probabilities  $P_S^i(0)$  and  $P_I^i(0)$  (with  $P_S^i(0) + P_I^i(0) = 1$ ), respectively.

According to dynamical rule Eq. (1) of the SIRP model, the transition kernel  $W_{\text{SIRP}}^i(\cdot)$  of the spreading process in layer  $a$  admits the following form

$$\begin{aligned} & W_{\text{SIRP}}^i(\tau_i^a, \omega_i^a, \varepsilon_i^a | \{\tau_k^a, \omega_k^a, \varepsilon_k^a\}_{k \in \partial_i^a}) \\ &= \mathbb{I}(\tau_i^a < \varepsilon_i^a) \left\{ P_I^i(0) \mathbb{I}(\tau_i^a = 0) + P_S^i(0) \mathbb{I}(\tau_i^a > 0) \prod_{t'=0}^{\tau_i^a-2} \prod_{k \in \partial_i^a} \mathbb{I}[1 - \beta_{ki} \mathbb{I}(\omega_k^a \geq t' + 1) \mathbb{I}(\tau_k^a \leq t')] \right. \\ & \quad \times \left[ 1 - \prod_{k \in \partial_i^a} [1 - \beta_{ki} \mathbb{I}(\omega_k^a \geq \tau_i^a) \mathbb{I}(\tau_k^a \leq \tau_i^a - 1)] \right] \times \left( \prod_{t''=\tau_i^a}^{\omega_i^a-2} (1 - \mu_i) \right) \mu_i \times \prod_{t'''=0}^{\tau_i^a-1} (1 - \gamma_i(t''')) \left. \right\} \\ & \quad + \mathbb{I}(\tau_i^a \geq \varepsilon_i^a) \left\{ P_S^i(0) \mathbb{I}(\tau_i^a > 0) \prod_{t'=0}^{\varepsilon_i^a-2} \prod_{k \in \partial_i^a} \mathbb{I}[1 - \beta_{ki} \mathbb{I}(\omega_k^a \geq t' + 1) \mathbb{I}(\tau_k^a \leq t')] \times \left[ \prod_{t''=0}^{\varepsilon_i^a-2} (1 - \gamma_i(t'')) \right] \gamma_i(\varepsilon_i^a - 1) \right\}. \end{aligned} \tag{A1}$$

The transition kernel  $W_{\text{LTM}}^i(\cdot)$  of the cascade process in layer  $b$  admits the following form

$$\begin{aligned} & W_{\text{LTM}}^i(\tau_i^b | \tau_i^a, \varepsilon_i^a, \{\tau_k^b\}_{k \in \partial_i^b}) \\ &= \mathbb{I} \left[ \sum_{k \in \partial_i^b} b_{ki} \mathbb{I}(\tau_k^b \leq \tau_i^b - 2) < \Theta_i \right] \delta_{\tau_i^b, \tau_i^a} + \mathbb{I}(\tau_i^b < \tau_i^a) \mathbb{I} \left[ \sum_{k \in \partial_i^b} b_{ki} \mathbb{I}(\tau_k^b \leq \tau_i^b - 2) < \Theta_i \right] \mathbb{I} \left[ \sum_{k \in \partial_i^b} b_{ki} \mathbb{I}(\tau_k^b \leq \tau_i^b - 1) \geq \Theta_i \right], \end{aligned} \tag{A2}$$

where the first term corresponds to the case where node  $i$  fails (in layer  $b$ ) due to infection (from layer  $a$ ), while the second term corresponds to the case where node  $i$  failed due to losing supports from neighboring nodes  $\partial_i^b$  in layer  $b$ .

For infection spread in layer  $a$ , the node-level probability of node  $i$  in a certain state is computed by tracing over the corresponding probabilities of trajectories  $m_a^{i \rightarrow j}(\cdot)$  (note that the process in layer  $b$  does not have a feedback influence

on layer  $a$ )

$$P_S^{i \rightarrow j}(t) = \sum_{\tau_i^a, \omega_i^a, \varepsilon_i^a} m_a^{i \rightarrow j}(\tau_i^a, \omega_i^a, \varepsilon_i^a) \mathbb{I}(t < \tau_i^a < \omega_i^a) \mathbb{I}(t < \varepsilon_i^a), \quad (\text{A3})$$

$$P_I^{i \rightarrow j}(t) = \sum_{\tau_i^a, \omega_i^a, \varepsilon_i^a} m_a^{i \rightarrow j}(\tau_i^a, \omega_i^a, \varepsilon_i^a) \mathbb{I}(\tau_i^a \leq t < \omega_i^a) \delta_{\varepsilon_i^a, \infty}, \quad (\text{A4})$$

$$P_R^{i \rightarrow j}(t) = \sum_{\tau_i^a, \omega_i^a, \varepsilon_i^a} m_a^{i \rightarrow j}(\tau_i^a, \omega_i^a, \varepsilon_i^a) \mathbb{I}(\tau_i^a < \omega_i^a \leq t) \delta_{\varepsilon_i^a, \infty}, \quad (\text{A5})$$

$$P_P^{i \rightarrow j}(t) = \sum_{\tau_i^a, \omega_i^a, \varepsilon_i^a} m_a^{i \rightarrow j}(\tau_i^a, \omega_i^a, \varepsilon_i^a) \mathbb{I}(\varepsilon_i^a \leq t) \delta_{\tau_i^a, \infty}. \quad (\text{A6})$$

The computation of these probabilities is similar to that of the SIR model, where we refer readers to Ref. [20] for the details.

For activities in layer  $b$ , the node-level probability of node  $i$  in state  $F$  (failed) is computed as

$$\begin{aligned} P_F^{i \rightarrow j}(t) &= \sum_{\tau_i^a, \omega_i^a, \varepsilon_i^a, \tau_i^b} \mathbb{I}(\tau_i^b \leq t) m_a^{i \rightarrow j}(\tau_i^a, \omega_i^a, \varepsilon_i^a, \tau_i^b) \\ &= \sum_{\tau_i^a, \omega_i^a, \varepsilon_i^a, \tau_i^b} \mathbb{I}(\tau_i^b \leq t) m_a^{i \rightarrow j}(\tau_i^a, \omega_i^a, \varepsilon_i^a) m_b^{i \rightarrow j}(\tau_i^b | \tau_i^a, \varepsilon_i^a) \end{aligned} \quad (\text{A7})$$

which appears much more difficult to treat due to the dependence on the activities in layer  $a$ . In particular, the failure of node  $i$  can be attributed to the infection from one of its neighbors from layer  $a$ , or to the failures of its neighbors from layer  $b$ . For the latter case, node  $i$  can be either in state  $S$  or in state  $P$  at time  $t$ , which depends on the infection time  $\tau_i^a$  and protection time  $\varepsilon_i^a$ . For this reason, we introduce the following conditional failure probability

$$\begin{aligned} P_F^{i \rightarrow j}(t | \tau_i^a, \omega_i^a, \varepsilon_i^a) &= \sum_{\tau_i^b} \mathbb{I}(\tau_i^b \leq t) m_b^{i \rightarrow j}(\tau_i^b | \tau_i^a, \varepsilon_i^a) = \sum_{\tau_i^b} \mathbb{I}(\tau_i^b \leq t) \frac{m_a^{i \rightarrow j}(\tau_i^a, \omega_i^a, \varepsilon_i^a, \tau_i^b)}{m_a^{i \rightarrow j}(\tau_i^a, \omega_i^a, \varepsilon_i^a)} \\ &= \mathbb{I}(\tau_i^a \leq t) + \mathbb{I}(\tau_i^a > t) \frac{\xi^{i \rightarrow j}(t | \tau_i^a, \omega_i^a, \varepsilon_i^a)}{m_a^{i \rightarrow j}(\tau_i^a, \omega_i^a, \varepsilon_i^a)}, \end{aligned} \quad (\text{A8})$$

where we have defined

$$\xi^{i \rightarrow j}(t | \tau_i^a, \omega_i^a, \varepsilon_i^a) := \mathbb{I}(\tau_i^a > t) \sum_{\tau_i^b} \mathbb{I}(\tau_i^b \leq t) m_b^{i \rightarrow j}(\tau_i^b | \tau_i^a, \omega_i^a, \varepsilon_i^a, \tau_i^b), \quad (\text{A9})$$

which is the cavity probability of node  $i$  not in state  $I$  or  $R$  but being failed at time  $t$  due to the failures of neighbors from layer  $b$ , while it follows the specific trajectory  $\{\tau_i^a, \omega_i^a, \varepsilon_i^a\}$  in layer  $a$ .

The marginal probability of node  $i$  in state  $F$  at time  $t$  is obtained by tracing over all the possible trajectories of layer  $a$  as

$$\begin{aligned} P_F^{i \rightarrow j}(t) &= \sum_{\tau_i^a, \omega_i^a, \varepsilon_i^a} \mathbb{I}(\omega_i^a > \tau_i^a) m_a^{i \rightarrow j}(\tau_i^a, \omega_i^a, \varepsilon_i^a) P_F^{i \rightarrow j}(t | \tau_i^a, \omega_i^a, \varepsilon_i^a) \\ &= P_I^{i \rightarrow j}(t) + P_R^{i \rightarrow j}(t) + \sum_{\tau_i^a, \omega_i^a, \varepsilon_i^a} \mathbb{I}(\tau_i^a > t) \mathbb{I}(\omega_i^a > \tau_i^a) \xi^{i \rightarrow j}(t | \tau_i^a, \omega_i^a, \varepsilon_i^a), \end{aligned} \quad (\text{A10})$$

where the summation in the last term can be further decomposed into  $P_{SF}^{i \rightarrow j}(t)$  and  $P_{PF}^{i \rightarrow j}(t)$ , depending on whether the protection on node  $i$  (given at time  $\varepsilon_i^a$ ) occurs after time  $t$  or before time  $t$

$$P_{SF}^{i \rightarrow j}(t) = \sum_{\tau_i^a, \omega_i^a, \varepsilon_i^a} \mathbb{I}(\varepsilon_i^a > t) \mathbb{I}(\tau_i^a > t) \mathbb{I}(\omega_i^a > \tau_i^a) \xi^{i \rightarrow j}(t | \tau_i^a, \omega_i^a, \varepsilon_i^a), \quad (\text{A11})$$

$$P_{PF}^{i \rightarrow j}(t) = \sum_{\tau_i^a, \omega_i^a, \varepsilon_i^a} \mathbb{I}(\varepsilon_i^a \leq t) \mathbb{I}(\tau_i^a > t) \mathbb{I}(\omega_i^a > \tau_i^a) \xi^{i \rightarrow j}(t | \tau_i^a, \omega_i^a, \varepsilon_i^a). \quad (\text{A12})$$

In summary, we can decompose  $P_F^{i \rightarrow j}(t)$  into four terms

$$P_F^{i \rightarrow j}(t) = P_I^{i \rightarrow j}(t) + P_R^{i \rightarrow j}(t) + P_{SF}^{i \rightarrow j}(t) + P_{PF}^{i \rightarrow j}(t), \quad (\text{A13})$$

where a similar form holds for  $P_F^i(t)$  as stated in the main text.

To obtain node-level iteration of  $P_{SF}^{i \rightarrow j}(t)$  and  $P_{PF}^{i \rightarrow j}(t)$ , the key is to further introduce the auxiliary probabilities  $\chi^{k \rightarrow i}(t)$ ,  $\psi^{k \rightarrow i}(t)$ ,  $\tilde{\chi}^{k \rightarrow i}(t, \varepsilon)$  and  $\tilde{\psi}^{k \rightarrow i}(t, \varepsilon)$ , defined as

$$\chi^{k \rightarrow i}(t) = \sum_{\tau_k^a, \omega_k^a, \varepsilon_k^a} \mathbb{I}(\omega_k^a > \tau_k^a) \prod_{t'=0}^{t-1} [1 - \beta_{ki} \mathbb{I}(\omega_k^a \geq t' + 1) \mathbb{I}(\tau_k^a \leq t')] m_a^{k \rightarrow i}(\tau_k^a, \omega_k^a, \varepsilon_k^a) P_F^{k \rightarrow i}(t-1 | \tau_k^a, \omega_k^a, \varepsilon_k^a), \quad (\text{A14})$$

$$\psi^{k \rightarrow i}(t) = \sum_{\tau_k^a, \omega_k^a, \varepsilon_k^a} \mathbb{I}(\omega_k^a > \tau_k^a) \prod_{t'=0}^{t-1} [1 - \beta_{ki} \mathbb{I}(\omega_k^a \geq t' + 1) \mathbb{I}(\tau_k^a \leq t')] m_a^{k \rightarrow i}(\tau_k^a, \omega_k^a, \varepsilon_k^a) \mathbb{I}(\tau_k^a \leq t-1), \quad (\text{A15})$$

$$\tilde{\chi}^{k \rightarrow i}(t, \varepsilon) = \sum_{\tau_k^a, \omega_k^a, \varepsilon_k^a} \mathbb{I}(\omega_k^a > \tau_k^a) \prod_{t'=0}^{\varepsilon-2} [1 - \beta_{ki} \mathbb{I}(\omega_k^a \geq t' + 1) \mathbb{I}(\tau_k^a \leq t')] m_a^{k \rightarrow i}(\tau_k^a, \omega_k^a, \varepsilon_k^a) P_F^{k \rightarrow i}(t-1 | \tau_k^a, \omega_k^a, \varepsilon_k^a), \quad (\text{A16})$$

$$\tilde{\psi}^{k \rightarrow i}(t, \varepsilon) = \sum_{\tau_k^a, \omega_k^a, \varepsilon_k^a} \mathbb{I}(\omega_k^a > \tau_k^a) \prod_{t'=0}^{\varepsilon-2} [1 - \beta_{ki} \mathbb{I}(\omega_k^a \geq t' + 1) \mathbb{I}(\tau_k^a \leq t')] m_a^{k \rightarrow i}(\tau_k^a, \omega_k^a, \varepsilon_k^a) \mathbb{I}(\tau_k^a \leq t-1). \quad (\text{A17})$$

These auxiliary probabilities are linked to  $P_{SF}^{i \rightarrow j}(t)$  and  $P_{PF}^{i \rightarrow j}(t)$  through the transition kernel  $W_{\text{SIRP}}^i$  and  $W_{\text{LTM}}^i$ , respectively, and their iteration equations can be mechanically derived (e.g., by relating  $\chi^{k \rightarrow i}(t)$  to  $\chi^{k \rightarrow i}(t-1)$ ). The explicit forms of the iteration equations and the physical interpretation of the auxiliary probabilities are stated in the main text.

## Appendix B: Deriving the Large-time Limit of the Discrete-time SIR Model

Here, we derive the DMP equations of the discrete-time SIR model in the large-time limit, which differs from the continuous-time counterpart [18].

We consider  $\gamma_i(t) = 0$  in Sec. III A and re-write the DMP equations for  $\theta^{i \rightarrow j}$  and  $\phi^{i \rightarrow j}$  as

$$\theta^{i \rightarrow j}(t+1) - \theta^{i \rightarrow j}(t) = -\beta_{ij} \phi^{i \rightarrow j}(t), \quad (\text{B1})$$

$$\phi^{i \rightarrow j}(t+1) - \phi^{i \rightarrow j}(t) = -(\beta_{ij} + \mu_i - \beta_{ij} \mu_i) \phi^{i \rightarrow j}(t) - [P_S^{i \rightarrow j}(t+1) - P_S^{i \rightarrow j}(t)]. \quad (\text{B2})$$

Summing both sides of the above equations from  $t = 0$  to  $t = T - 1$  and canceling the term  $\sum_{t=0}^{T-1} \phi^{i \rightarrow j}(t)$  yields

$$\phi^{i \rightarrow j}(T) - \phi^{i \rightarrow j}(0) = \frac{\beta_{ij} + \mu_i - \beta_{ij} \mu_i}{\beta_{ij}} [\theta^{i \rightarrow j}(T) - \theta^{i \rightarrow j}(0)] - [P_S^{i \rightarrow j}(T) - P_S^{i \rightarrow j}(0)]. \quad (\text{B3})$$

Define  $p_{ij} = \beta_{ij} / (\beta_{ij} + \mu_i - \beta_{ij} \mu_i)$  and remind that the initial conditions for the messages are  $P_S^{i \rightarrow j}(0) = P_S^i(0)$ ,  $\phi^{i \rightarrow j}(0) = 1 - P_S^i(0)$ ,  $\theta^{i \rightarrow j}(0) = 1$ , which leads to

$$\theta^{i \rightarrow j}(T) = 1 - p_{ij} + p_{ij} P_S^{i \rightarrow j}(T) + p_{ij} \phi^{i \rightarrow j}(T). \quad (\text{B4})$$

When  $T \rightarrow \infty$ , all infected nodes will recover, which implies that  $\phi^{i \rightarrow j}(\infty) = 0$  and leads to the self-consistent equations for the messages  $\theta^{i \rightarrow j}$  as

$$\begin{aligned} \theta^{i \rightarrow j}(\infty) &= 1 - p_{ij} + p_{ij} P_S^{i \rightarrow j}(\infty) \\ &= 1 - p_{ij} + p_{ij} P_S^i(0) \prod_{k \in \partial_i^a \setminus j} \theta^{k \rightarrow i}(\infty). \end{aligned} \quad (\text{B5})$$

## Appendix C: Resource Capacity Constraint in Mirror Descent

When designing algorithms for mitigating network failure, we impose the realistic resource capacity constraint in the form of

$$\sum_{i \in V_b} \sum_{t=0}^{T-1} \gamma_i(t) \leq \gamma^{\text{tot}}. \quad (\text{C1})$$



Such a linear equality constraint can generally be handled by introducing a Lagrangian multiplier and deriving the corresponding Karush-Kuhn-Tucker condition (KKT condition), or by introducing a barrier function as in the interior point method. Consider the latter approach by augmenting the objective function with a log barrier function as

$$f(\gamma) := \gamma^{\text{tot}} - \sum_{i \in V_b} \sum_{t=0}^{T-1} \gamma_i(t), \quad (\text{C2})$$

$$\mathcal{O}_{\text{aug}}(\gamma) := \mathcal{O}(\gamma) - \lambda \cdot \log(f(\gamma)), \quad (\text{C3})$$

where  $\lambda > 0$  is a tunable parameter. The log barrier function strongly penalizes  $\mathcal{O}_{\text{aug}}(\gamma)$  when  $f(\gamma)$  is close to zero, which encourages  $\gamma$  to stay in the interior of the feasible region of Eq. (C1).

The gradient of the augmented objective function reads

$$\nabla_{\gamma} \mathcal{O}_{\text{aug}}(\gamma) = \nabla_{\gamma} \mathcal{O}(\gamma) + \frac{\lambda}{f(\gamma)} \mathbf{1}, \quad (\text{C4})$$

where  $\mathbf{1}$  is the all-one vector. Eq. (C4) suggests a global shift of the gradient to encourage the satisfaction of the capacity constraint. This is the motivation for considering a shifted gradient  $g^n = \nabla_{\gamma} \mathcal{O}(\gamma^n) - b^n$  in the mirror descent algorithm in the main text. The gradient shift  $-b^n$  is toggled on when  $\sum_{t,i} \gamma_i^n(t) \lesssim \gamma^{\text{tot}}$ , where the shift magnitude  $b^n$  is chosen based on the following arguments

$$\gamma^{n+1} = \Psi^{-1}(\Psi(\gamma^n) - s \cdot [\nabla_{\gamma} \mathcal{O}(\gamma^n) - b^n]), \quad (\text{C5})$$

$$\begin{aligned} \sum_{t,i} \gamma_i^{n+1}(t) &\approx \sum_{t,i} \Psi^{-1}(\Psi(\gamma_i^n(t))) - s \sum_{t,i} \Psi^{-1'}(\Psi(\gamma_i^n(t))) \left[ \frac{\partial}{\partial \gamma_i(t)} \mathcal{O}(\gamma^n) - b^n \right] \\ &= \sum_{t,i} \gamma_i^n(t) - s \sum_{t,i} \gamma_i^n(t) (1 - \gamma_i^n(t)) \left[ \frac{\partial}{\partial \gamma_i(t)} \mathcal{O}(\gamma^n) - b^n \right] \lesssim \gamma^{\text{tot}}, \end{aligned} \quad (\text{C6})$$

where a small step size  $s$  is assumed. It requires that

$$\sum_{t,i} \gamma_i^n(t) (1 - \gamma_i^n(t)) \left[ \frac{\partial}{\partial \gamma_i(t)} \mathcal{O}(\gamma^n) - b^n \right] \approx 0, \quad (\text{C7})$$

$$\iff b^n \approx \frac{\sum_{t,i} \gamma_i^n(t) (1 - \gamma_i^n(t)) \frac{\partial}{\partial \gamma_i(t)} \mathcal{O}(\gamma^n)}{\sum_{t,i} \gamma_i^n(t) (1 - \gamma_i^n(t))}, \quad (\text{C8})$$

which explains the choice of  $b^n$  in the main text.

#### Appendix D: Online Supply of Resources

In this appendix, we consider the cases where the resources arrive in an online fashion, e.g., a limited number of vaccines can be produced every day. In these cases, there is a resource capacity constraint  $\gamma_t^{\text{tot}}$  at each time step  $t$ , yielding the following constrained optimization problems

$$\min_{\gamma} \mathcal{O}(\gamma) = \frac{1}{N} \sum_{i \in V_b} P_F^i(T), \quad (\text{D1})$$

$$\text{s. t. } 0 \leq \gamma_i(t) \leq 1 \quad \forall i, t, \quad (\text{D2})$$

$$\sum_{i \in V_b} \gamma_i(t) \leq \gamma_t^{\text{tot}} \quad \forall t. \quad (\text{D3})$$

The mirror descent algorithm introduced in Sec. V A can be readily applied to solve this optimization problem, except that the shifted gradient  $g_t^n = \nabla_{\gamma(t)} \mathcal{O}(\gamma^n(t)) - b_t^n$  has a time-dependent shift  $b_t^n$  in this case. The shift magnitude  $b_t^n$  at time  $t$  can be derived in the same spirit as in Appendix. C, which admits the following expression

$$b_t^n \approx \frac{\sum_i \gamma_i^n(t) (1 - \gamma_i^n(t)) \frac{\partial}{\partial \gamma_i(t)} \mathcal{O}(\gamma^n)}{\sum_i \gamma_i^n(t) (1 - \gamma_i^n(t))}. \quad (\text{D4})$$

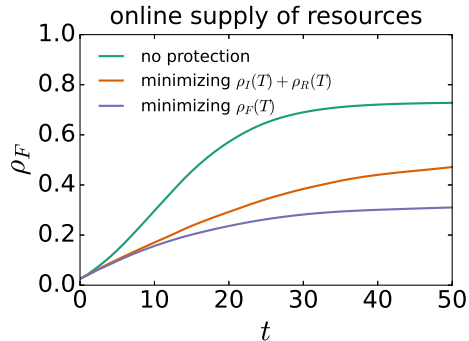


Figure 8. Evolution of the size of failures  $\rho_F(t)$  of the synthetic network shown in Fig. 6 under various mitigation strategies. The time window is set as  $T = 50$ . The system parameters are  $\beta_{ji} = 0.17$ ,  $\mu = 0.5$ ,  $\Theta_i = 0.6|\partial_i^b|$ . Planted influence parameters  $\{b_{ji}\}$  are considered. Three nodes are randomly chosen as the initially infected individuals, and  $\gamma_t^{\text{tot}} = 2$  is considered.

If the resource capacity constraint for  $\gamma_t^{\text{tot}}$  is still violated, we project the control variables at time  $t$  to the feasible region through a simple rescaling

$$\gamma^n(t) \leftarrow \frac{\gamma_t^{\text{tot}}}{\sum_i \gamma_i^n(t)} \gamma^n(t). \quad (\text{D5})$$

As a concrete example, we consider the synthetic two-layer network in Sec. V C using the planted influence parameters  $\{b_{ji}\}$  as in Fig. 7(b). The results are shown in Fig. 8, which illustrates the effectiveness of the optimization algorithms for the scenario with the online supply of resources.

### Appendix E: Probabilistic Seeding

There are some cases where the initial infection status of a node  $i$  is not fully determined but follows a probability distribution  $P_j^i(0)$ , which may be obtained after some inference. In the DMP framework, we simply use the available  $\{P_j^i(0)\}$  as the initial condition to iterate the DMP equations, and further optimize the evolution by deploying the protection resources.

we consider a similar setting as in Sec. V B. In Fig. 5, there are 3 seeds, each of which has  $P_j^i(0) = 1$ . In this section, we consider 6 seeds, each of which has  $P_j^i(0) = \frac{1}{2}$ . The results of optimization are shown in Fig. 9. It can be observed that the optimization algorithm can still successfully reduce the final failure size, as in the cases with deterministic seeding. Interestingly, the optimal protection resource distribution  $\{\gamma_i^*(t)\}$  is also concentrated among a few nodes at a certain time step (as shown in Fig. 9(c) and (d)), even though one cannot be sure about which nodes are initially infected. This may be due to the simple network topology, where there exists a clear optimal deployment strategy to block the infections coming from the 6 probabilistic seeds altogether, as shown in Fig. 9(e) and (f).

- 
- [1] Anton Pak, Oyelola A. Adegboye, Adeshina I. Adekunle, Kazi M. Rahman, Emma S. McBryde, and Damon P. Eisen, “Economic consequences of the covid-19 outbreak: the need for epidemic preparedness,” *Frontiers in Public Health* **8** (2020).
  - [2] Kunal Chaturvedi, Dinesh Kumar Vishwakarma, and Nidhi Singh, “Covid-19 and its impact on education, social life and mental health of students: A survey,” *Children and Youth Services Review* **121**, 105866 (2021).
  - [3] Abigail L. Cochran, “Impacts of covid-19 on access to transportation for people with disabilities,” *Transportation Research Interdisciplinary Perspectives* **8**, 100263 (2020).
  - [4] Zhitao Xu, Adel Elomri, Laoucine Kerbache, and Abdelfatteh El Omri, “Impacts of covid-19 on global supply chains: Facts and perspectives,” *IEEE Engineering Management Review* **48**, 153–166 (2020).
  - [5] Serpil Aday and Mehmet Seckin Aday, “Impact of COVID-19 on the food supply chain,” *Food Quality and Safety* **4**, 167–180 (2020).
  - [6] M. Hadi Amini, Hamidreza Arasteh, and Pierluigi Siano, “Sustainable smart cities through the lens of complex interdependent infrastructures: Panorama and state-of-the-art,” in *Sustainable Interdependent Networks II*:

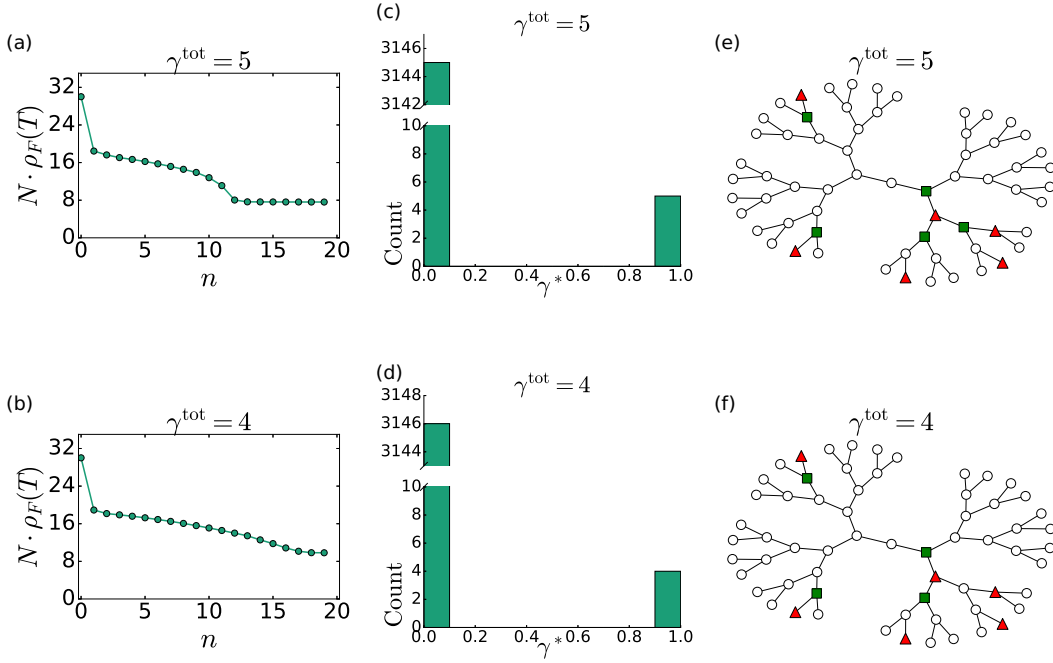


Figure 9. Mitigation of the network failures in a binary tree network of size  $N = 63$  for both layers. Panels (a)(c)(e) correspond to the case with  $\gamma^{\text{tot}} = 5$ , while Panels (b)(d)(f) correspond to the case with  $\gamma^{\text{tot}} = 4$ . Panels (a) and (b) depict how the final failure size changes during the optimization process. Panels (c) and (d) plot the histogram of the optimal decision variables  $\{\gamma_i^*(t)\}$ . Panels (e) and (f) show the optimal placement of resources, where green square nodes receive protection (having a high  $\gamma_i^*(t)$  at time  $t = 0$ ). The six red triangle nodes are the potential seeds for infection, each of which has an initial infection probability  $P_i^i(0) = \frac{1}{2}$ .

*From Smart Power Grids to Intelligent Transportation Networks*, edited by M. Hadi Amini, Kianoosh G. Boroojeni, S. S. Iyengar, Panos M. Pardalos, Frede Blaabjerg, and Asad M. Madni (Springer International Publishing, Cham, 2019) pp. 45–68.

- [7] Xin Liu, Bo Chen, Chen Chen, and Dong Jin, “Electric power grid resilience with interdependencies between power and communication networks - a review,” *IET Smart Grid* **3**, 182–193.
- [8] Hengdao Guo, Ciyan Zheng, Herbert Ho-Ching Iu, and Tyrone Fernando, “A critical review of cascading failure analysis and modeling of power system,” *Renewable and Sustainable Energy Reviews* **80**, 9–22 (2017).
- [9] Brian Karrer and M. E. J. Newman, “Competing epidemics on complex networks,” *Phys. Rev. E* **84**, 036106 (2011).
- [10] Weiran Cai, Li Chen, Fakhteh Ghanbarnejad, and Peter Grassberger, “Avalanche outbreaks emerging in cooperative contagions,” *Nature Physics* **11**, 936–940 (2015).
- [11] Wei Wang, Quan-Hui Liu, Junhao Liang, Yanqing Hu, and Tao Zhou, “Coevolution spreading in complex networks,” *Physics Reports* **820**, 1–51 (2019), coevolution spreading in complex networks.
- [12] Hanlin Sun, David Saad, and Andrey Y. Lokhov, “Competition, collaboration, and optimization in multiple interacting spreading processes,” *Phys. Rev. X* **11**, 011048 (2021).
- [13] Sergey V. Buldyrev, Roni Parshani, Gerald Paul, H. Eugene Stanley, and Shlomo Havlin, “Catastrophic cascade of failures in interdependent networks,” *Nature* **464**, 1025–1028 (2010).
- [14] Amir Bashan, Yehiel Berezin, Sergey V. Buldyrev, and Shlomo Havlin, “The extreme vulnerability of interdependent spatially embedded networks,” *Nature Physics* **9**, 667–672 (2013).
- [15] Romualdo Pastor-Satorras, Claudio Castellano, Piet Van Mieghem, and Alessandro Vespignani, “Epidemic processes in complex networks,” *Rev. Mod. Phys.* **87**, 925–979 (2015).
- [16] David Adam, “Special report: The simulations driving the world’s response to COVID-19,” *Nature* **580**, 316–318 (2020).
- [17] Wei Wang, Ming Tang, H Eugene Stanley, and Lidia A Braunstein, “Unification of theoretical approaches for epidemic spreading on complex networks,” *Reports on Progress in Physics* **80**, 036603 (2017).
- [18] Brian Karrer and M. E. J. Newman, “Message passing approach for general epidemic models,” *Phys. Rev. E* **82**, 016101 (2010).
- [19] Andrey Y. Lokhov, Marc Mézard, Hiroki Ohta, and Lenka Zdeborová, “Inferring the origin of an epidemic with a dynamic message-passing algorithm,” *Phys. Rev. E* **90**, 012801 (2014).
- [20] Andrey Y. Lokhov, Marc Mézard, and Lenka Zdeborová, “Dynamic message-passing equations for models with unidirectional dynamics,” *Phys. Rev. E* **91**, 012811 (2015).
- [21] Andreas Koher, Hartmut H. K. Lentz, James P. Gleeson, and Philipp Hövel, “Contact-based model for epidemic spreading on temporal networks,” *Phys. Rev. X* **9**, 031017

- (2019).
- [22] Bo Li and David Saad, “Impact of presymptomatic transmission on epidemic spreading in contact networks: A dynamic message-passing analysis,” *Phys. Rev. E* **103**, 052303 (2021).
- [23] Andrey Lokhov, “Reconstructing parameters of spreading models from partial observations,” in *Proceedings of the 30th International Conference on Neural Information Processing Systems*, Vol. 29, edited by D. Lee, M. Sugiyama, U. Luxburg, I. Guyon, and R. Garnett (Curran Associates Inc., Red Hook, NY, USA, 2016) pp. 3467 – 3475.
- [24] Andrey Y. Lokhov and David Saad, “Optimal deployment of resources for maximizing impact in spreading processes,” *Proceedings of the National Academy of Sciences* **114**, E8138–E8146 (2017).
- [25] S. Boccaletti, G. Bianconi, R. Criado, C.I. del Genio, J. Gómez-Gardeñes, M. Romance, I. Sendiña-Nadal, Z. Wang, and M. Zanin, “The structure and dynamics of multilayer networks,” *Physics Reports* **544**, 1–122 (2014), the structure and dynamics of multilayer networks.
- [26] Duncan J. Watts, “A simple model of global cascades on random networks,” *Proceedings of the National Academy of Sciences* **99**, 5766–5771 (2002).
- [27] David Kempe, Jon Kleinberg, and Éva Tardos, “Maximizing the spread of influence through a social network,” in *Proceedings of the Ninth ACM SIGKDD International Conference on Knowledge Discovery and Data Mining*, KDD '03 (Association for Computing Machinery, New York, NY, USA, 2003) pp. 137–146.
- [28] Zhen Su and Jürgen Kurths, “A dynamic message-passing approach for social contagion in time-varying multiplex networks,” *Europhysics Letters* **123**, 68004 (2018).
- [29] F. Altarelli, A. Braunstein, L. Dall’Asta, and R. Zecchina, “Large deviations of cascade processes on graphs,” *Phys. Rev. E* **87**, 062115 (2013).
- [30] Marc Mézard and Andrea Montanari, *Information, Physics, and Computation* (Oxford University Press, Oxford, 2009).
- [31] Giuseppe Torrisi, Alessia Annibale, and Reimer Kühn, “Overcoming the complexity barrier of the dynamic message-passing method in networks with fat-tailed degree distributions,” *Phys. Rev. E* **104**, 045313 (2021).
- [32] Munik Shrestha, Samuel V. Scarpino, and Cristopher Moore, “Message-passing approach for recurrent-state epidemic models on networks,” *Phys. Rev. E* **92**, 022821 (2015).
- [33] P. Grassberger, “On the critical behavior of the general epidemic process and dynamical percolation,” *Mathematical Biosciences* **63**, 157–172 (1983).
- [34] J Chalupa, P L Leath, and G R Reich, “Bootstrap percolation on a bethe lattice,” *Journal of Physics C: Solid State Physics* **12**, L31 (1979).
- [35] Jiaying Zhou, Yi Zhao, and Yong Ye, “Complex dynamics and control strategies of SEIR heterogeneous network model with saturated treatment,” *Physica A: Statistical Mechanics and its Applications* **608**, 128287 (2022).
- [36] Atılım Günes Baydin, Barak A. Pearlmutter, Alexey Andreyevich Radul, and Jeffrey Mark Siskind, “Automatic differentiation in machine learning: A survey,” *J. Mach. Learn. Res.* **18**, 5595–5637 (2017).
- [37] Qianxiao Li, Long Chen, Cheng Tai, and Weinan E, “Maximum principle based algorithms for deep learning,” *Journal of Machine Learning Research* **18**, 1–29 (2018).
- [38] A.S. Nemirovski and D.B. Yudin, *Problem Complexity and Method Efficiency in Optimization* (Wiley, New York, 1983).
- [39] Amir Beck and Marc Teboulle, “Mirror descent and non-linear projected subgradient methods for convex optimization,” *Oper. Res. Lett.* **31**, 167–175 (2003).
- [40] R. Christie, “Power systems test case archive, university of washington,” Available at: [https://labs.ece.uw.edu/pstca/pf118/pg\\_tca118bus.htm](https://labs.ece.uw.edu/pstca/pf118/pg_tca118bus.htm) (1993).
- [41] Ye Cai, Yong Li, Yijia Cao, Wenguo Li, and Xiangjun Zeng, “Modeling and impact analysis of interdependent characteristics on cascading failures in smart grids,” *International Journal of Electrical Power & Energy Systems* **89**, 106–114 (2017).